A systematic approach to obtaining numerical solutions of Jeffery's type equations using Spherical Harmonics

S. Montgomery-Smith[a], David A. Jack[b], Douglas E. Smith[c]

[a]*Department of Mathematics, University of Missouri, Columbia MO 65211, U.S.A.*
[b]*Department of Mechanical Engineering, Baylor University, Waco, TX 76798, U.S.A.*
[c]*Department of Mechanical and Aerospace Engineering, University of Missouri, Columbia MO 65211, U.S.A.*

Abstract

This paper extends the work of Bird, Warner, Stewart, Sørensen, Larson, Ottinger, Vukadinovic, and Forest *et al.*, who have applied Spherical Harmonics to numerically solve certain types of partial differential equations on the two-dimensional sphere. We present a systematic approach and implementation for solving such equations with efficient numerical solutions. In particular we are able to solve a wide variety of fiber orientation equations considered before by Jeffery, Folgar and Tucker, and Koch, and include several recently introduced fiber orientation collision models. The main tools used to compute the coefficients for the Spherical Harmonic-based expansion are Rodrigues' formula and the ladder operators. We show that solutions of the Folgar-Tucker model using our new algorithm retains the accuracy of full simulations of the fiber orientation distribution function with computational efforts that are only slightly more than the Advani-Tucker orientation/moment tensor solutions commonly used in industrial applications. The spherical harmonic approach requires a computational effort of just three times that of the orientation tensor approach employing the orthotropic closure of VerWeyst, but with less than 1/1000th the computational effort of numerical solutions of the full orientation distribution function obtained using control volume methods.

Keywords: Jeffery's equation, spherical harmonic, anisotropic diffusion, fiber orientation

1. Introduction

Computations involving the equation of motion for a probability distribution function defined on the unit sphere have received increased interest in recent years. Notable applications include those that model short-fiber reinforced polymer processing (see, *e.g.*, [1]), crystalline polymers (see, *e.g.*, [2, 3, 4]), turbulence (see, *e.g.*, [5]), nanofibers (see, *e.g.*, [6]) and aerosol transport (see, *e.g.*, [7]). This paper focuses on a Spherical Harmonics Galerkin expansion approach to evaluate the inclusion orientation probability distribution function as expressed in the diffusion equation by Bird *et al.* [8] also known as a modified Fokker-Planck equation or the Smoluchowski equation (see, *e.g.*, [9]), with particular emphasis on representations of short fiber orientation kinematics for concentrated suspensions.

Among published short fiber orientation distribution simulation approaches, few enjoy the widespread acceptance of the Folgar and Tucker [1] model which forms the basis for most

industrial fiber orientation simulations today (see, *e.g.*, [10, 11, 12, 13]). Recent experiments by Nguyen and co-workers [14], however, have exposed previously unknown limitations of the Folgar-Tucker model, raising questions on the appropriate form to define the orientation diffusion (see, *e.g.*, [15, 16, 17, 18, 19, 20]). The solution procedure considered in the present work makes it possible to quickly implement and solve the Folgar and Tucker model and many of its generalized forms that address issues associated with orientation diffusion, as well as enhanced forms that are yet to be developed. Results are presented below for solutions to the Folgar and Tucker model, and for solutions employing anisotropic rotary diffusion such as that of the Koch [15] model, the model of Phelps and Tucker [20], and the reduced-strain closure model of Wang *et al.* [19].

Numerical solutions of the fiber orientation distribution function for even simple flow problems require a relatively large computational effort to evaluate the equations of motion. For example, obtaining the transient solution of the complete fiber orientation distribution function in a simple injected molded center-gated disk can take days to weeks on a standard workstation (see, *e.g.*, [21, 13]), thus rendering such evaluations ineffective for engineering design purposes. To cast these probability distributions in an acceptable industrial form, Advani and Tucker [10] simplified calculations using moments of the orientation distribution function written as orientation tensors. This technique yields a tensor expression for the equation of motion (see, *e.g.*, Equation (36) below), thus replacing the partial differential equation of motion for the probability distribution with an ordinary differential equation for the moments of the distribution. The orientation tensor approach is widely employed in industry to predict the orientation state of concentrated suspensions (see, *e.g.*, [22, 11, 12, 23, 24, 25, 13]). The industrial case of a center-gated disk can be solved on the order of minutes for the second- and the fourth-order moment tensor equations of motion (see, *e.g.*, Jack and Smith [13]).

The evolution equation of each even-ordered orientation tensor requires that the next higher even-ordered orientation tensor be available. In practice, the solution process is truncated or 'closed' by approximating the orientation tensor of a particular order in terms of the lower-ordered tensors. For example, there exist many closure approximations of the fourth-order orientation tensor which are evaluated as a function of the second-order orientation tensor (see, *e.g.*, [26, 2, 10, 21, 27, 12, 23, 24, 25]), and there are several closures which approximate the sixth-order orientation tensor written in terms of the fourth-order orientation tensor ([10, 22, 13, 28]). Lipscomb *et al.* [29] demonstrated approaches to avoid the use of closure approximations by solving an 'equivalent strain tensor', but these approaches are only valid in the range of dilute concentrations and are thus discarded in the present study for concentrated suspensions.

Unfortunately, simulations that rely on orientation tensor closures yield truncated approximations to the solution of the fiber orientation distribution function. In fact, each tensor closure method can be shown to exhibit limitations under certain flow conditions, either in the quantitative numerical results or remaining within the 'physical' realm of possible orientation states, and thus are inherently suspect. Jack and Smith [30] considered the relative effect of a closure on the truncation error. They showed that all fourth and sixth-order closures are, respectively, limited by the fourth, and sixth-order spherical harmonic based reconstructions of the orientation distribution function, and that further work on the closures of the fourth-order orientation tensor will only serve to have nominal increases in

computational accuracy. More importantly, it is always uncertain as to the effectiveness of a particular closure developed for one class of partial differential equations in the setting of a similar, but fundamentally different, constitutive equation. The Spherical Harmonics-based approach presented here eliminates the need for orientation tensors and their related closures. As such, closure methods are included here for comparison purposes only where it is shown that our approach enjoys the computational accuracy of full orientation distribution function simulations, while retaining computational efficiencies similar to that of the orientation tensor closure methods.

The orientation state of short fibers is of interest during processing, but for the product designer it is often the composite's structural performance that is of interest. Advani and Tucker [10] presented an orientation averaging procedure to relate the fourth-order orientation tensor obtained from a mold filling simulation to the material stiffness tensor of the molded part. Jack and Smith [31] demonstrated through the use of the Spherical Harmonics, that only fourth-order moments of the orientation distribution function are required to compute the expectation of the material stiffness as all higher order moments integrate to zero due to orthogonality. In addition, Jack and Smith [32] showed that the predicted expectation of the material stiffness tensor from forth-order orientation tensors provides reasonable results as compared to those obtained from numerical simulations of the full fiber orientation distribution function. Jack and Smith [31] also evaluted the variance of the elasticity tensor which requires moments of the orientation distribution function beyond the forth order. Current orientation tensor based approaches for processing predictions include up to the fourth-order tensor moments only, and thus would be unable to capture any higher order structural properties such as the stiffness variance or plastic deformation characteristics.

Spherical Harmonic-based methods for solving partial differential equations on the unit sphere have been presented elsewhere (see, *e.g.*, [33, 34, 8, 35, 36, 6, 37]). Vukadinovic [37] investigated the inertial manifolds of the Smoluchowski equation for colloidal suspensions and used Spherical Harmonics to transform the system to eliminate the gradient from the nonlinear term in the differential equation. Recently Forest *et al.* [6] developed an efficient solver using a spherical harmonic Galerkin expansion of the Smoluchowski equation. They moved beyond the traditional second-order spherical harmonic expansion employed in [33, 2, 38, 36, 39] to expansions up to the 65th order to represent orientation.

The present work moves beyond that of Forest *et al.* [6] by forming the spherical harmonic expansion of any order for a wide variety of general rotary diffusions, applicable to a wide range of colloidal suspension flows: from short fibers to nano-composites to liquid-crystalline polymers. We provide a systematic numerical approach to the solution procedure so that it can be easily adapted to other more general situations as evidenced by the examples provided below.

We also mention other related papers. Onat [40] and Onat and Leckie [41] presented spherical harmonic expansions of probability distribution functions on the unit sphere up to the fourth-order to evaluate the elastic moduli of a material with penny- shaped voids. A similar method was later used by Advani and Tucker [10] for expansions of the distribution function to evaluate elastic properties of short-fiber composites. Jack and Smith [30] used the method of spherical harmonic expansions as a basis for comparing transient orientation solutions obtained using closures of various order, and presented the analytic form for the sixth-order expansion. Recently, Jack and Smith [31] used a spherical harmonic expansion to

derive analytic expressions for the expectation and variance of the elastic property tensor for short-fiber polymer composites which required the orientation moment tensors up through the eighth-order.

2. Differential Equations on the Unit Sphere

The objective of this paper is to present a systematic spherical harmonic method to numerically solve partial differential equations on the two dimensional sphere, $S = \{\mathbf{r} = (x, y, z) : |\mathbf{r}|^2 = x^2+y^2+z^2 = 1\}$, or in spherical coordinates, $\mathbf{r} = (x, y, z) = (\sin\theta\cos\phi, \sin\theta\sin\phi, \cos\theta)$, where $0 \leq \theta \leq \pi$, $0 \leq \phi \leq 2\pi$. The partial differential equations considered here are of the form

$$\frac{\partial}{\partial t}\psi = F(\mathbf{r}, \boldsymbol{\nabla})\psi, \tag{1}$$

where ψ is a function (for example, the orientation probability distribution function) defined on S. Here F is a polynomial in six variables, with the proviso that it matters in which order the terms of each monomial part are written. We believe that this includes many of the published, if not all, of the partial differential equations that describe the evolution of the orientation distribution function for short fiber suspensions.

Here $\boldsymbol{\nabla}$ denotes the gradient operator restricted to the sphere, not the usual gradient in three-dimensional space, that is:

$$\boldsymbol{\nabla} = (\nabla_x, \nabla_y, \nabla_z) = \boldsymbol{\theta}\frac{\partial}{\partial\theta} + \csc\theta\boldsymbol{\phi}\frac{\partial}{\partial\phi} = (I - \mathbf{rr}) \cdot \left(\frac{\partial}{\partial x}, \frac{\partial}{\partial y}, \frac{\partial}{\partial z}\right) \tag{2}$$

where

$$\boldsymbol{\theta} = (\cos\theta\cos\phi, \cos\theta\sin\phi, -\sin\theta) \tag{3}$$

$$\boldsymbol{\phi} = (-\sin\phi, \cos\phi, 0) \tag{4}$$

The spherical harmonic approach converts Equation (1) to a system of ordinary differential equations written as

$$\frac{\partial}{\partial t}\hat{\psi}_l^m = \sum_{l'=0}^{\infty}\sum_{m'=-l'}^{l'} c_{l,l'}^{m,m'}\hat{\psi}_{l'}^{m'}, \tag{5}$$

where $\hat{\psi}_l^m$ ($l \geq 0$, $|m| \leq l$) are the spherical harmonic coefficients of ψ, given in Equation (19), with the coefficients $c_{l,l'}^{m,m'}$ defined in Equation (25). Larson [35] obtained the coefficients for the non-linear terms, but this is beyond the scope of the present study.

The main focus of this paper is to develop a systematic algorithm for calculating the coefficients $c_{l,l'}^{m,m'}$ appearing in Equation (5) (and also in Equation (25) below). This algorithm makes it possible to readily solve all differential equations on the unit sphere of the form shown in Equation (1), and specifically the fiber orientation distribution equation given in Bird *et al.* [8]. With this systematic approach, we hope to open up this method to a much wider audience. The approach presented here offers three advantages: 1) using the algorithm, the experimentalist can easily try new partial differential equations that purportedly models their situation, 2) if the order of the Spherical Harmonics is taken high enough, one can obtain arbitrarily high accuracy (indeed, because the Spherical Harmonics

form a Hilbert basic sequence, it will likely be easy to estimate the numerical error), and 3) the matrices of coefficients $c_{l,l'}^{m,m'}$ in equation (5) are surprisingly sparse, and as such, the numerical algorithm lends itself to rapid computations.

3. Description of the Model Equations

To illustrate our solution method, we consider variations of Jeffery's equation [42] which describes the motion of fibers in a moving fluid with vorticity $\mathbf{w}$ and rate of deformation tensor Γ. Jeffery's equation is often written in terms of the fiber orientation distribution function ψ and the fiber aspect ratio parameter $-1 \leq \lambda \leq 1$ as

$$\frac{\partial}{\partial t}\psi = J\psi := -\tfrac{1}{2}\boldsymbol{\nabla} \cdot (\mathbf{w} \times \mathbf{r}\psi + \lambda(\Gamma \cdot \mathbf{r} - \Gamma : \mathbf{rrr})\psi), \tag{6}$$

where we note that the right hand side is in the form of Equation (1). A variation of Equation (6) incorporates the rotary diffusion expressed by Bird *et al.* [8], occasionally referred to as the generalized Fokker-Planck or the Smoluchowski equation [9], as

$$\frac{\partial}{\partial t}\psi = J\psi + \boldsymbol{\nabla} \cdot \boldsymbol{\nabla}(D_r\psi), \tag{7}$$

where D_r captures the effect of fiber interaction and depends upon the flow kinetics. Folgar and Tucker [1] selected $D_r = C_I\gamma$ where $\gamma = \left(\frac{1}{2}\Gamma : \Gamma\right)^{1/2}$ and C_I is a constant that depends upon the volume fraction and aspect ratio of the fibers.

To better illustrate our systematic approach, we include the solution of Equations (6) and (7) in the examples below, even though they have been solved previously with Spherical Harmonics using the coefficients $c_{l,l'}^{m,m'}$ in Equation (5) that appear in Bird and Warner [34].[] In our analysis, we will also consider examples of anisotropic diffusion such as that proposed by Koch [15] in the differential equation

$$\frac{\partial}{\partial t}\psi = J\psi + \boldsymbol{\nabla} \cdot (I - \mathbf{rr}) \cdot D_r \cdot \boldsymbol{\nabla}\psi = J\psi + (\boldsymbol{\nabla} - 2\mathbf{r}) \cdot D_r \cdot \boldsymbol{\nabla}\psi \tag{8}$$

where the anisotropic diffusion matrix D_r is defined in terms of the model parameters C_1 and C_2 (see Koch [15] for more detail) as

$$D_r = C_1\gamma^{-1}(\Gamma : \mathbb{A} : \Gamma)I + C_2\gamma^{-1}\Gamma : \mathcal{A} : \Gamma. \tag{9}$$

In the above, the $(I - \mathbf{rr})$ term, with I being the identity tensor, serves to project vectors onto the surface of the sphere. We note that this term is not explicitly included in Koch's [15] formula, however it's existence is implied in the original introduction.

The anisotropic diffusion matrix D_r defined in Equation (9) is written in terms of the 2nd, 4th and 6th order moment tensors of ψ which are, respectively, defined as

$$A := \int_S \psi\mathbf{rr}\, d\mathbf{r}, \qquad \mathbb{A} := \int_S \psi\mathbf{rrrr}\, d\mathbf{r}, \qquad \text{and} \qquad \mathcal{A} := \int_S \psi\mathbf{rrrrrr}\, d\mathbf{r}. \tag{10}$$

In these integrals, we adopt the common definition for the integral of a function $F(\mathbf{r})$ over the surface of the unit sphere as

$$\int_S F(\mathbf{r})\, dr := \int_{\theta=0}^{\pi} \int_{\phi=0}^{2\pi} F(\mathbf{r}) \sin\theta \, d\phi \, d\theta, \tag{11}$$

and we note here that the moment tensors A, $\mathbb{A}$, and $\mathcal{A}$ can be expressed in terms of Spherical Harmonics as shown below in Equation (34).

Phelps and Tucker [20] proposed a slightly different form of D_r, the "anisotropic rotary diffusion", which is written in terms of the fitted parameters $b_i, i = 1, 2, \ldots 5$ as

$$D_r = b_1\gamma I + b_2\gamma A + b_3\gamma A^2 + \tfrac{1}{2}b_4\Gamma + \tfrac{1}{4}b_5\gamma^{-1}\Gamma^2. \tag{12}$$

Note that the constants $\frac{1}{2}$ and $\frac{1}{4}$ in Equation (12) are modified from that given in the formula by Phelps and Tucker [20] since they use $\frac{1}{2}\Gamma$ for the rate of deformation tensor.

Before developing our Spherical Harmonics solution method, it is helpful to consider additional mathematical relationships that will be used below. Care must be exercised in not confusing the differential geometry on the surface of the sphere S with the differential geometry in the three dimensional space $\mathbb{R}^3$ it is embedded in. Thus, for example, integration by parts is the slightly unexpected form

$$\int_S \mathbf{f} \cdot \boldsymbol{\nabla} g \, d\mathbf{r} = -\int_S (\boldsymbol{\nabla} \cdot (I - \mathbf{rr}) \cdot \mathbf{f}) g \, d\mathbf{r} = \int_S ((2\mathbf{r} - \boldsymbol{\nabla}) \cdot \mathbf{f}) g \, d\mathbf{r}, \tag{13}$$

where the gradient operator $\boldsymbol{\nabla}$ is restricted to orientation space as defined in Equation (2). Equation (13) reduces to the usual integration by parts when $\mathbf{f}$ is tangential to the surface of the sphere. We also recall the so called angular momentum operator

$$\mathbf{L} = -i\mathbf{r} \times \boldsymbol{\nabla} = (L_x, L_y, L_z) = -i\left(y\frac{\partial}{\partial z} - z\frac{\partial}{\partial y}, z\frac{\partial}{\partial x} - x\frac{\partial}{\partial z}, x\frac{\partial}{\partial y} - y\frac{\partial}{\partial x}\right), \tag{14}$$

where, as usual, i denotes the complex number satisfying $i^2 = -1$. Integration by parts for the angular momentum operator is more straightforward, that is,

$$\int_S \mathbf{f} \cdot \mathbf{L} g \, d\mathbf{r} = -\int_S (\mathbf{L} \cdot \mathbf{f}) g \, d\mathbf{r}. \tag{15}$$

Note that $\mathbf{L} \times \mathbf{L} = \boldsymbol{\nabla} \times \boldsymbol{\nabla} = i\mathbf{L}$, and in particular ∇_x, ∇_y and ∇_z do not commute with each other. We also use the formulae $\mathbf{r} \cdot \boldsymbol{\nabla} f = \mathbf{r} \cdot \mathbf{L} f = \mathbf{L} \cdot (\mathbf{r} f) = 0$ and $\boldsymbol{\nabla} \cdot (\mathbf{r} f) = 2f$. For completeness, the proof of Equations (13) and (15) in given in the Appendix.

4. Spherical Harmonics Solutions

A brief description of Spherical Harmonics is given here to provide much of the background needed to apply our solution procedure. The interested reader is encouraged to review Weisstein [43] or similar for further details.

Any square integrable function ψ defined on S may be written as a Fourier series like representation in terms of the Spherical Harmonics $Y_l^m(\theta,\phi)$ for $l \geq 0$ and $|m| \leq l$ as

$$\psi = \sum_{l=0}^{\infty} \sum_{m=-l}^{l} \hat{\psi}_l^m Y_l^m, \tag{16}$$

where we can define the Spherical Harmonics as

$$Y_l^m(\theta,\phi) = \sqrt{\frac{(2l+1)(l-m)!}{4\pi(l+m)!}} P_l^m(\cos\theta) e^{im\phi}. \tag{17}$$

Both $Y_l^m(\theta,\phi)$ and their complex conjugates $\bar{Y}_l^m(\theta,\phi) = Y_l^m(\theta,-\phi) = (-1)^m Y_l^{-m}(\theta,\phi)$ are written as functions of the associated Legendre Polynomials defined as

$$P_l^m(z) = \frac{(-1)^{l+m}}{2^l l!}(1-z^2)^{m/2} \frac{\partial^{l+m}}{\partial z^{l+m}}(1-z^2)^l. \tag{18}$$

The coefficients $\hat{\psi}_l^m$ in Equation (16) are evaluated from

$$\hat{\psi}_l^m = \int_S \psi \bar{Y}_l^m d\mathbf{r}, \tag{19}$$

We note that the spherical harmonic functions form an orthogonal basis, i.e.,

$$\int_S Y_l^m \bar{Y}_{l'}^{m'} \, d\mathbf{r} = \delta_{l,l'}\delta_{m,m'} \tag{20}$$

where $\delta_{i,j}$ is the Kronecker delta.

Note that Equation (16) has been used in rigid-inclusion applications for reconstructions of the fiber orientation probability distribution from the moment tensors (see, *e.g.*, [10, 30]), and for analytical forms of the stiffness tensor expectation and variance from the moment tensors [31]. In both cases, the series for ψ in Equation (16) was truncated at a relatively low order (that is, $l = 2$, 4, or 8) rather than retaining the complete series.

To obtain the system of ordinary differential Equations (5), we integrate Equation (1) against $\bar{Y}_l^m$ over the unit sphere to obtain its adjoint or weak form as

$$\frac{\partial}{\partial t} \int_S \psi \bar{Y}_l^m \, d\mathbf{r} = \int_S \psi F^*(\mathbf{r}, \boldsymbol{\nabla}) \bar{Y}_l^m \, d\mathbf{r}, \tag{21}$$

where the right hand side follows from integration by parts and F^* denotes any polynomial F in which each monomial term is written in reverse order with the substitution $2\mathbf{r} - \boldsymbol{\nabla}$ for $\boldsymbol{\nabla}$. Therefore, applying Equation (21), Jeffery's Equation (6) is defined by

$$J^* = \tfrac{1}{2}(\mathbf{w} \cdot (\mathbf{r} \times \boldsymbol{\nabla}) + \lambda \mathbf{r} \cdot \Gamma \cdot \boldsymbol{\nabla}), \tag{22}$$

Similarly, the two extensions of Jeffery's equation that include diffusion appearing in Equations (7) and (8) (expressed as $\frac{\partial}{\partial t}\psi = F\psi$), respectively become

$$F^* = J^* + D_r \boldsymbol{\nabla} \cdot \boldsymbol{\nabla}, \tag{23}$$

and

$$F^* = J^* + (\boldsymbol{\nabla} - 2\mathbf{r}) \cdot D_r \cdot \boldsymbol{\nabla}. \tag{24}$$

In all cases, we can decompose

$$F^*(\mathbf{r}, \boldsymbol{\nabla}) \bar{Y}_l^m = \sum_{l'=0}^{\infty} \sum_{m'=-l'}^{l'} c_{l,l'}^{m,m'} \bar{Y}_{l'}^{m'}, \tag{25}$$

and therefore obtain the spherical harmonic representation shown in Equation (5) above.

The difficulty in solving Equation (1) is therefore reduced to computing the coefficients $c_{l,l'}^{m,m'}$ in Equation (25). For this, we need to evaluate the effect of differentiating and multiplying by x, y or z on the Spherical Harmonics function in Eq. (17). First we consider Rodrigues' formula which describes the effect of multiplying any Y_l^m by z giving

$$zY_l^m = \sqrt{\frac{(l+m)(l-m)}{(2l-1)(2l+1)}} Y_{l-1}^m + \sqrt{\frac{(l+m+1)(l-m+1)}{(2l+1)(2l+3)}} Y_{l+1}^m. \tag{26}$$

The angular momentum operators in Equation (14) are used to define ladder operators

$$\begin{aligned} L_+ &= L_x + iL_y = e^{i\phi} \left(\frac{\partial}{\partial \theta} + i \cot\theta \frac{\partial}{\partial \phi} \right), \\ L_- &= L_x - iL_y = e^{-i\phi} \left(-\frac{\partial}{\partial \theta} + i \cot\theta \frac{\partial}{\partial \phi} \right), \end{aligned} \tag{27}$$

so called because of how they effect the Spherical Harmonics, that is,

$$\begin{aligned} L_+ Y_l^m &= \sqrt{(l-m)(l+m+1)} Y_l^{m+1}, \\ L_- Y_l^m &= \sqrt{(l+m)(l-m+1)} Y_l^{m-1}. \end{aligned} \tag{28}$$

It can also be shown that

$$L_z Y_l^m = m Y_l^m. \tag{29}$$

It follows that the effect of multiplying by polynomials in x and y can be evaluated from the identities

$$x = -i[L_y, z] \quad \text{and} \quad y = i[L_x, z], \tag{30}$$

respectively, where $[U, V]$ denotes the commutator $UV - VU$. Similarly, applying the gradient operator follows from

$$\nabla_x = ziL_y - yiL_z, \quad \nabla_y = xiL_z - ziL_x, \quad \nabla_z = yiL_x - xiL_y. \tag{31}$$

Then using Equations (26) to (31), it is possible to compute explicitly the coefficients $c_{l,l'}^{m,m'}$ in Equation (25), and hence the same in Equation (5). It is helpful to note that in certain special cases, calculations can be simplified by applying

$$\boldsymbol{\nabla} \cdot \boldsymbol{\nabla} Y_l^m = -l(l+1) Y_l^m \tag{32}$$

which holds for Spherical Harmonics by design since they are constructed as eigenfunctions of the Laplacian operator.

Moment tensors may be computed using Spherical Harmonics as well. For example, to compute the 6th order moment tensor $\mathcal{A}$ in Equation (10) we simply expand

$$\mathbf{rrrrrr}\bar{Y}_0^0 = \sum_{l=0}^{6}\sum_{m=-l}^{l} \mathcal{C}_{l,m}\bar{Y}_l^m, \tag{33}$$

where $\mathcal{C}_{l,m}$ is the tensor of rank six composed of coefficients calculated by applying x, y and z to $\bar{Y}_0^0$ six times using the Rodrigues' formula and ladder operators described above. It follows that since $\bar{Y}_0^0 = 1/\sqrt{4\pi}$, the 6th order orientation tensor becomes

$$\mathcal{A} = \sqrt{4\pi}\int_S \psi\mathbf{rrrrrr}\bar{Y}_0^0\, d\mathbf{r} = \sqrt{4\pi}\sum_{l=0}^{6}\sum_{m=-l}^{l} \mathcal{C}_{l,m}\hat{\psi}_l^m, \tag{34}$$

where the orthogonality of the Spherical Harmonics are used to simplify the final result.

5. The "Spherical" Program Algorithm

An automated algorithm has been implemented to compute the coefficients $c_{l,l'}^{m,m'}$ in Equation (25) for any differential equation satisfying the criteria given above (and, therefore, the $\mathcal{C}_{l,m}$ in Equation (34)). The algorithm recursively applies the replacement rules described in Equation (35) until no further substitutions can be made. Here "op" denotes any of z, L_z, L_+, or L_- operations, and $\mathcal{Y}$ denotes any linear combination of the $\bar{Y}_l^m$'s. We are compute the effect the complex conjugates have on the Spherical Harmonics, thus the formulae are slightly different than those derived above.

$$\begin{aligned}
\mathrm{op}(\mathcal{Y} \pm c\bar{Y}_l^m) &\to \mathrm{op}(\mathcal{Y}) \pm c\,\mathrm{op}(\bar{Y}_l^m),\\
x\mathcal{Y} &\to ziL_y(\mathcal{Y}) - iL_y(z\mathcal{Y}),\\
y\mathcal{Y} &\to iL_x(z\mathcal{Y}) - ziL_x(\mathcal{Y}),\\
z\bar{Y}_l^m &\to \sqrt{\frac{(l+m)(l-m)}{(2l-1)(2l+1)}}\bar{Y}_{l-1}^m + \sqrt{\frac{(l+m+1)(l-m+1)}{(2l+1)(2l+3)}}\bar{Y}_{l+1}^m,\\
\nabla_x\mathcal{Y} &\to ziL_y(\mathcal{Y}) - yiL_z(\mathcal{Y}),\\
\nabla_y\mathcal{Y} &\to xiL_z(\mathcal{Y}) - ziL_x(\mathcal{Y}),\\
\nabla_z\mathcal{Y} &\to yiL_x(\mathcal{Y}) - xiL_y(\mathcal{Y}),\\
L_x(\mathcal{Y}) &\to \tfrac{1}{2}\left(L_+(\mathcal{Y}) + L_-(\mathcal{Y})\right),\\
L_y(\mathcal{Y}) &\to -\tfrac{i}{2}\left(L_+(\mathcal{Y}) - L_-(\mathcal{Y})\right),\\
L_z\bar{Y}_l^m &\to -m\bar{Y}_l^m,\\
L_+\bar{Y}_l^m &\to -\sqrt{(l+m)(l-m+1)}\bar{Y}_l^{m-1},\\
L_-\bar{Y}_l^m &\to -\sqrt{(l-m)(l+m+1)}\bar{Y}_l^{m+1}
\end{aligned} \tag{35}$$

It is important to note that $x\bar{Y}_l^m$, $y\bar{Y}_l^m$, $z\bar{Y}_l^m$, $\nabla_x\bar{Y}_l^m$, $\nabla_y\bar{Y}_l^m$, and $\nabla_z\bar{Y}_l^m$ involve $\bar{Y}_{l'}^{m'}$ for l' and m' that differ from l and m, respectively, by at most one. [1]

6. The Reduced Strain Closure Model

To further illustrate the flexibility of our solution procedure, we consider the recently proposed reduced strain closure model for fiber orientation calculations by Wang *et al.* [19]. Their approach is based on the orientation tensor method [10] where a differential equation is derived by applying orientation averaging to Equation (1). The governing equation for the second moment tensor A is written in terms of F^* in Equation (23) as

$$\frac{\partial}{\partial t}A = B := \int_S \psi F^*(\mathbf{r}, \boldsymbol{\nabla})(\mathbf{rr})\, d\mathbf{r}. \tag{36}$$

For example, Phelps and Tucker [20] showed that if ψ is a probability distribution satisfying Equation (8), then the following holds:

$$\begin{aligned}\frac{\partial}{\partial t}A =& \tfrac{1}{2}(W\cdot A - A\cdot W + \lambda(A\cdot\Gamma + \Gamma\cdot A - 2\mathbb{A}:\Gamma)) \\ &+ 2D_r - 2(\mathrm{tr}D_r)A - 5(A\cdot D_r + D_r\cdot A) + 10\mathbb{A}:D_r,\end{aligned} \tag{37}$$

where $W = \begin{bmatrix} 0 & -w_3 & w_2 \\ w_3 & 0 & -w_1 \\ -w_2 & w_1 & 0 \end{bmatrix}$.

Note that the moment tensor Equation (37) is of particular interest since Wang *et al.* [19] noted that experimental evidence showed overwhelmingly that the rotary diffusivity in Equation (7) over-estimates the rate of alignment for a concentrated suspension of fibers in pure shearing flows. They apply a simple modification to delay alignment by rewriting the evolution equation for A as $\dot{A} = \kappa B$ where κ is the so called "strain reduction factor" taking values of $0 \le \kappa \le 1$.

Unfortunately, the strain reduction factor approach suffers from the disadvantage that it is not objective. Hence Wang *et al.* [19] proposed the RSC model which slows orientation alignment in simulations of A while remaining objective. To solve the RSC model using our spherical harmonic approach we first write A in its spectral form $A = \sum_{k=1}^{3}\lambda_k\mathbf{e}_k\mathbf{e}_k$, where the λ_k are the eigenvalues, and the $\mathbf{e}_k$ are the corresponding orthonormal eigenvectors. Then Equation (36) can be rewritten as

$$\sum_{k=1}^{3}(\dot{\lambda}_k\mathbf{e}_k\mathbf{e}_k + \lambda_k\dot{\mathbf{e}}_k\mathbf{e}_k + \lambda_k\mathbf{e}_k\dot{\mathbf{e}}_k) = B,$$

[1] The developed script employed in the present study uses the recursive algorithm in Equation (35) to create threaded functions in the programming language C which in turn are used in an iterative procedure for computing the solution to the differential equation in Equation (1). The script may be found at `http://www.math.missouri.edu/~stephen/software/spherical` and is written in perl making use of either the commercial computer algebra system Mathematica by Wolfram Research, or the open-source computer algebra system Maxima. The scripts are designed to work in a Unix like environment.

from which it follows that $\dot{\lambda}_k = \mathbf{e}_k\mathbf{e}_k : B$, and a similar explicit formula for $\dot{\mathbf{e}}_k$ exists. The RSC model replaces the equations for $\dot{\lambda}_k$ with

$$\dot{\lambda}_k^{\text{new}} = \kappa \mathbf{e}_k\mathbf{e}_k : B,$$

but leaves the equations for $\dot{\mathbf{e}}_k$ intact. Thus the RSC model equation for $\dot{A}$ is

$$\frac{\partial}{\partial t}A^{\text{new}} = B - (1-\kappa)\sum_{k=1}^{3}\dot{\lambda}_k\mathbf{e}_k\mathbf{e}_k = B - (1-\kappa)\mathbb{M} : B, \tag{38}$$

where $\mathbb{M}$ is the rank four tensor $\sum_{k=1}^{3}\mathbf{e}_k\mathbf{e}_k\mathbf{e}_k\mathbf{e}_k$. It follows that the RSC model for ψ is

$$\frac{\partial}{\partial t}\psi^{\text{new}} = F - (1-\kappa)G + H \tag{39}$$

where

$$G = \tfrac{15}{8\pi}(\mathbf{rr} - \tfrac{1}{5}I) : \mathbb{M} : B = \tfrac{1}{4\pi}(\text{tr}B) - \tfrac{5}{8\pi}\boldsymbol{\nabla}\cdot((\mathbb{M} : B)\cdot\mathbf{r} - (\mathbb{M} : B) : \mathbf{rrr}). \tag{40}$$

In the above equations, H is any quantity whose second moments are zero.

7. Numerical Examples

We first consider the example of Jeffery's equation without diffusion as expressed in Equation (6). The motivation to use Jeffery's equation as our first example is two fold: 1) there are explicit solutions with which we can compare our numerics, and 2) the solutions to Jeffery's equation can contain sharp peaks with almost shock-like characteristics, and hence can be regarded as a tough work-out for the numerical methods. Indeed, the addition of diffusion will smooth the data, and hence render the numerics easier.

To ensure adequate results for our example simulations, we consider Spherical Harmonics of order $L = 400$. It can be shown that there are L^2 Spherical Harmonics of order less than or equal to L, and since each coefficient is a complex number, this means that analysis with $L = 400$ yields a system of ordinary differential equations with $320,000$ dependent variables. In this case this is computationally unrealistic since directly computing Equation (5) requires multiplications with a $320,000 \times 320,000$ matrix, that is, about one hundred billion operations.

Fortunately, there are several attributes that significantly reduce the size of the matrix equations for this problem, making it more tractable with regard to computational efforts. It can be shown that if F^* is a polynomial of degree at most d, then $c_{l,l'}^{m,m'}$ is non-zero only if both $|l - l'| \leq d$ and $|m - m'| \leq d$. For the Jeffery's Equation (6), F^* is of degree 2 which reduces the matrix multiplications to include matrices with only $25 \times 320,000$ non-zero entries. We do not distinguish between the "back" and "front" of each fiber, further reducing the computational effort. To incorporate this fiber symmetry, we identify antipodal points, that is, $\mathbf{r}$ with $-\mathbf{r}$, or equivalently, (θ, ϕ) with $(-\theta, \phi+\pi)$. Thus in the decomposition Equation (16), $\hat{\psi}_l^m$ is non-zero only when l is even, which reduces the number of coefficients by a factor of approximately two. Also, the functions ψ are real valued, yielding an additional

two-fold redundancy in the coefficients since $\hat{\psi}_l^{-m} = (-1)^m \bar{\hat{\psi}}_l^m$. Therefore, the matrices in Equation (5) for Jeffery's Equation (6) with order $L = 400$ requires multiplications with matrices that are approximately $15 \times 80,000$ in size which is trivially solved in any standard programming language.

A pure shearing flow is considered, defined by vorticity $\mathbf{w} = (0, 0, -G)$ and rate of deformation $\Gamma = \begin{bmatrix} 0 & G & 0 \\ G & 0 & 0 \\ 0 & 0 & 0 \end{bmatrix}$. This models a fluid undergoing shear parallel to the yz-plane, where the amount of shear is equal to Gx and is in the y direction. It has been shown that the fiber orientation tensor solution for a dilute suspension is periodic with period corresponding to a fiber rotating through 180° of $2\pi/G\sqrt{1-\lambda^2}$ (see, *e.g.*, [38]).

Figure 1 shows numerical results for selected entries of the second moment tensor, A_{11}, A_{22}, A_{33} and A_{12}, beginning from an initially isotropic orientation state (that is, $\psi = 1/4\pi$ at $t = 0$) with $\lambda = 0.98$. Values appearing in Figure 1 result from simulations with Spherical Harmonics of order 400. The systems of ordinary differential equations in Equation (5) were computed using the Adams-Bashforth method of order 4 with a time step size of 10^{-3}. The result is periodic with the correct period, that is $31.57/G$. It is important to note that simulations with a significantly lower order of Spherical Harmonics (i.e., $L = 200$) produced results that were of a lower quality (not shown). Current industrial simulations for predicting fiber orientation within a processed part employ the orientation tensor approach of Advani and Tucker [10], which requires a closure approximation. To provide a comparison with the orientation tensor-based approach and the Spherical Harmonic approach, we provide additional results in Figure 1 for solutions using the orientation tensor equation of motion with the Hybrid and the ORT closures. It is common practice to use the Hybrid closure [10] due to its computational efficiency, or one of the fitted orthotropic closures (see, *e.g.* [12, 44, 24, 45]) when higher accuracy is needed. In particular, the ORT closure of VerWeyst *et al.* [45] has found widespread acceptance and it is important here to relate the solutions from our Spherical Harmonics solution approach to the orientation tensor-based method that employ closure approximations. Solutions of second-order orientation tensor equation of motion using the aforementioned closures are shown in Figure 1, and it is clear that solutions from the ORT and the Spherical Harmonics approach yield visually identical solutions, whereas the Hybrid closure differs considerably. Of note is the predicted period from the ORT closure, $31.72/G$, is not the same as the true Jeffery period, but is nonetheless impressive considering the solution relies on an approximation of $\mathbb{A}$.

Figure 2 illustrates numerical results for two flows modeled with the Folgar-Tucker diffusion model of Equation (7) with $C_I = 10^{-3}$. Here we consider a pure elongational flow given by $\mathbf{w} = (0, 0, 0)$ and $\Gamma = \begin{bmatrix} 2G & 0 & 0 \\ 0 & -G & 0 \\ 0 & 0 & -G \end{bmatrix}$, and the pure shear flow discussed above with $\lambda = 1$. We solve the system with the Adams-Bashforth method of order 2, a time step size of 10^{-3} and a spherical harmonic expansion of order $L = 100$. Results for the spherical harmonic solution are denoted by $A_{ij}^{\text{Spherical}}$ and are compared with numerical results from the full orientation Distribution Function Calculation (DFC) using the control volume method suggested by Bay [46]. This comparison is performed due to the widespread acceptance of the accuracy of Bay's approach (see, *e.g.*, [12, 24, 13]). As observed in Figure 2, the results from the two approaches are graphically indistinguishable, and observations of the numerical outputs shows identical solutions between the two methods out to the fourth and fifth significant digits. Similar studies were performed over a variety of flow conditions (not shown

here), and results from the two approaches yield numerically identical solutions. Simulations are also presented in Figure 2 for solutions of A using the orientation tensor approach with the ORT and the Hybrid closures to approximate the fourth-order orientation tensor. It is clear from Figure 2(b) that the results from the closures do not approach the accuracy of the Spherical Harmonic approach. The DFC approach and the Spherical Harmonic approach yield identical solutions, but it is important to mention that the usefulness of the DFC approach is limited due to the excessively large computational expense required for solutions. The computational resources for the DFC increase exponentially as either the degree of fiber interaction diminishes in the Folgar and Tucker model (i.e. $C_I \downarrow 0$) or as the diffusion model for the form of D_r becomes more complex. Thus obtaining results using the DFC approach for pure Jeffery's motion from the previous example would be well beyond our available computational resources. This limitation is avoided with the Spherical Harmonic approach as solution accuracy is only limited by machine precision, but have similar computational overheads as the industrially accepted closure approach.

As with other series representations, a small error is introduced when truncating the Spherical Harmonics expansion to order L. It is desired that the resulting truncation error is within a tolerable level while avoiding the computational burden associated with retaining unnecessary higher-order terms. To this end, we truncated Equation (5) at various Lth order expressions, and solved Jeffery's equation with Folgar-Tucker diffusion of Equation (7) for the aforementioned elongational and shearing flows. The results with various orders of expansion appear in Figure 3. As seen in the elongational flow results in Figure 3(a), the lower order expansion ($L = 20$) maintains the correct solution throughout the initial aligning stages, but once the orientation distribution nears an aligned state, the solution begins to rapidly diverge. As L increases, the spherical harmonic approach is better equipped to represent a highly aligned orientation state. Notice in this case that the A_{11} component approaches 0.9975 (recall, $A_{11} = 1$ is unidirectional in the x direction) requiring that the order of the expansion be increased to properly represent the highly aligned condition. Notice that an expansion of $L = 100$ is quite sufficient in our elongational flow simulations. Higher degrees of alignment (that is, those resulting from lower C_I values) are expected to require a higher order expansion to avoid unstable solutions. Conversely, the shearing flow does not experience an orientation state as aligned as in the elongational flow. Notice in Figure 3(b) that $L = 30$ is nearly indistinguishable from the case $L = 400$, and that $L = 50$ has been found to work well in all flows with $C_I = 10^{-3}$ where the shearing component of the flow dominates over the elongational component (such flows prevent a high degree of alignment).

The results presented above demonstrate that the spherical harmonic approach yields solutions with an accuracy equal to solutions using the control volume approach of Bay [46] and well beyond that of the orientation tensor approach. Unfortunately, accuracy alone is not sufficient for industrial implementation. To this end, several simulations were performed to compare the computational effort required to obtain fiber orientation states with the Folgar-Tucker diffusion model using the spherical harmonic approach, the orientation tensor approach, and the control volume approach. A normalized time t_{Norm} is defined as the number of seconds of computer processing time required to solve for a unit of flow evolution time for the flow (that is, $\Delta t = G^{-1}$). Computations were performed on a Dual Zeon, 3.6 GHz processor running in 32-bit mode with 4 GB of RAM using multi-threading for all three solution methods. The control volume results (DFC) were obtained using a variation of Bay's

[46] code written in Fortran 95 and multi-threaded using Intel's compiler. The orientation tensor results were obtained using an in-house code, and the closure approximations were evaluated using highly optimized algorithms. Each of the three simulation methods were used to compute fiber orientation in all of the 13 flow conditions that includes various combinations of shearing and elongational flows as described in Jack and Smith [13]. It can be shown that the flows selected encompass the eigenspace of A and they have served to demonstrate both the effectiveness and the limitations of a particular closure under different flow conditions (see, *e.g.*, [12, 44, 24, 13]).

The results from the analysis are summarized in Table 1. For each of the approaches, three normalized time values are given, the maximum, the minimum and the average over each of the flow simulations. The reason for the variation in the orientation tensor approaches of the ORT, Hybrid, Spherical ($L = 50$) and Spherical ($L = 100$) is partially attributed to the accuracy of the system clock used (clock precision $\sim 10^{-3}$) and the fact that the compiled results will behave differently based on the different flow types since different components of the velocity gradient tensor will be zero under each of the flows. On the other hand, the DFC time variations are directly attributed to the velocity field since the step size employed is a function of the scalar magnitude of the rate of deformation, which is different for each of the flows investigated.

Notice that the control volume approach is clearly the slowest method averaging over 800 seconds of computational time to solve just one second of flow time. Conversely, the spherical harmonic approach (with order $L = 50$) requires three orders of magnitude less computational effort than the control volume solution approach. As discussed previously, the 50th order expansion is adequate for shearing and shearing dominated flows, and it is evident from Table 1 that it requires just over 3 times the computational effort of the orientation tensor approach using the ORT closure. This is important, since our spherical harmonic approach computes a fiber orientation solution to an accuracy previously available only through the computationally prohibitive control volume simulations of the orientation distribution function, but with the computational expense comparable to the orientation tensor approach.

There is another interesting aspect to the spherical harmonic approach lending to a greater robustness. A common point of concern with the control volume class of solutions stems from the inherent spatial discretizing effect, which causes parts of the sphere that lie along the boundaries of the mesh to be weighted unequally. In particular, meshes that treat the "north" and "south" poles specially (for example, spherical coordinate finite meshes) will be particularly susceptible. On the other hand, the function space spanned by Spherical Harmonics is invariant under rotations of the sphere.

Next we consider calculations using the recently proposed orientation diffusion model of Koch [15]. Solutions using the DFC approach are not presented as they would have required computational efforts on the order of months to solve, and in particular they would yield the identical numerical results as the Spherical Harmonic approach which is solved on the order of seconds. Solutions using the orientation tensor approach are not considered either since the second-order orientation tensor equation of motion for the Koch model requires a second- to sixth-order closure (cf. the EBF closure of Jack and Smith [28]) and since Phelps and Tucker [20] showed that these solutions are prone to yield non-physical results. Figure 4 shows the results of Jeffery's equation with the Koch type diffusion [15] (cf. Equations (8)

and (9)), with $C_1 = 0.0021$, $C_2 = 0.075$, and $\lambda = 1$ for the same shear flow described above. This is a rather difficult case to model, because A_{11} approaches 0.934, which nears perfect alignment. Note that this case was considered by Phelps and Tucker [20], which in their Figure 2 corresponds to a volume fraction of fibers of $v_f = 0.01$. We choose this particular scenario to present since Phelps and Tucker were unable to produce physical results (that is, A_{11} became greater than one) due to limitations of the closure methods they employed. We solved the same problem using Spherical Harmonics of order $L = 100$, and compared the answer to Spherical Harmonics of order $L = 200$.

We also consider the Folgar-Tucker diffusion combined with the reduced-strain closure model described in Equations (39) and (40) above and results are illustrated in Figure 5. We use the same parameters as given in Figure 4 of Wang *et al.* [19], namely $C_I = 0.01$, and $\kappa = 0.1$. Finally, Figure 6 shows Spherical Harmonics simulation results using the Phelps-Tucker anisotropic rotary diffusion (cf. Equations (8) and (12)) combined with the reduced-strain closure model described in Equation (37). We use the same parameters as given in Figure 5 of Phelps and Tucker [20], namely $b_1 = 1.924 \times 10^{-4}$, $b_2 = 5.839 \times 10^{-3}$, $b_3 = 4.0 \times 10^{-2}$, $b_4 = 1.168 \times 10^{-5}$, $b_5 = 0$, and $\kappa = 1/30$. In all these examples, we used the same shear flow described above with $\lambda = 1$, and Spherical Harmonics of order 50. In each of these cases, we obtain results similar to the literature, but certainly not identical. This difference is due to the methods employed in the literature, which rely on a moment tensor closure approach thus only approximating the solution. As demonstrated above, the spherical harmonic approach lends itself to accurate solutions provided the expansion truncation is taken sufficiently large enough, as was done in each of the proceeding examples. Thus the results from the spherical harmonic expansion can be considered 'exact' if the expansion is taken sufficiently high.

8. Conclusions

We believe that the spherical harmonic method provides both speed and accuracy, that it might either displace, or at least complement, the use of moment tensor closures in many industrial settings. Results demonstrate that the Spherical Harmonic approach may retain an accuracy only limited by machine precision, thus surpassing the moment tensor approach which requires an approximation for higher order information. We provide a systematic approach, so workers in the field should be able to quickly develop software to solve the particular differential equations that they wish to investigate.

9. Acknowledgements

The authors gratefully acknowledge support from N.S.F. via grant C.M.M.I. 0727399. They are also extremely grateful to various attendees of the XVth International Congress on Rheology/Society of Rheology 80th Annual Meeting, who brought many references of prior work to their attention. The authors which to express their gratitude to Professor Charles Tucker III of the University of Illinois at Urban-Champaign for providing us with the highly efficient code to solve the ORT closure, which we further optimized for our compilers. We also wish to express our gratitude to Dr. Tucker for his help in understanding his recent RSC and ARD diffusion models. In particular, the first named author wishes to acknowledge the

influence of the paper Phelps and Tucker [20], which clarified to him the importance of the $(I - \mathbf{rr})$ term in the Koch model.

Appendix A. Integration by Parts on the Sphere

Here we indicate a possible approach to proving Equations (13) and (15). Although the approach we present is not "slick" (for example, using ideas from differential geometry such as Stokes' formula), we have found the presented approach to be rather concrete and reliable.

The idea is to consider any sequence of differentiable functions $\theta_n : [0, \infty) \to [0, \infty)$ such that for bounded continuous functions f, we have $\int_0^\infty f(x)\theta_n(x)\, dx \to f(1)$ as $n \to \infty$, and $\theta_n(x)$ is zero for x sufficiently close to zero and n sufficiently large. For example, $\theta_1(x) = \frac{1}{2}x^2 e^{-x}$, and $\theta_n(x) = n\theta_1(n(x-1)+1)$ if $x > 1 - \frac{1}{n}$ and zero otherwise.

Then we note that

$$\int_S f(\mathbf{r})\, d\mathbf{r} = \lim_{n\to\infty} \int_{\mathbb{R}^3} f\left(\frac{\mathbf{r}}{|\mathbf{r}|}\right) \theta_n(|\mathbf{r}|)\, d\mathbf{r}, \tag{A.1}$$

where the right hand side is the usual triple integral over $\mathbf{r} = (x, y, z)$. Then in this new context, we define

$$\boldsymbol{\nabla} f(\mathbf{r}) = |\mathbf{r}| \left(I - \frac{\mathbf{rr}}{|\mathbf{r}|^2}\right) \cdot \frac{\partial}{\partial \mathbf{r}} f(\mathbf{r}), \tag{A.2}$$

where $\frac{\partial}{\partial \mathbf{r}}$ denotes the standard gradient operator in three dimensions. This formula is designed so that if f is homogeneous of degree zero, that is, $f(\mathbf{r}) = f(\mathbf{r}/|\mathbf{r}|)$, then $\boldsymbol{\nabla} f$ is also homegenous of degree zero. Then Equation (13) follows from

$$\int_{\mathbb{R}^3} \mathbf{f}\left(\frac{\mathbf{r}}{|\mathbf{r}|}\right) \cdot \boldsymbol{\nabla} g\left(\frac{\mathbf{r}}{|\mathbf{r}|}\right) \theta_n(|\mathbf{r}|)\, d\mathbf{r} = \int_{\mathbb{R}^3} \left(\left(2\frac{\mathbf{r}}{|\mathbf{r}|} - \boldsymbol{\nabla}\right) \cdot \mathbf{f}\left(\frac{\mathbf{r}}{|\mathbf{r}|}\right)\right) g\left(\frac{\mathbf{r}}{|\mathbf{r}|}\right) \theta_n(|\mathbf{r}|)\, d\mathbf{r}. \tag{A.3}$$

This is a laborious but elementary computation, using the usual one dimensional integration by parts. There are terms involving θ_n' but these disappear at the end of the calculation.

Equation (15) is accomplished via Equation (13), setting $\mathbf{L}f(\mathbf{r}) = -i|\mathbf{r}|^{-1}\mathbf{r} \times \boldsymbol{\nabla} f(\mathbf{r})$, and noticing that $\mathbf{L}f(\mathbf{r}) = i\boldsymbol{\nabla} \times (|\mathbf{r}|^{-1}\mathbf{r} f(\mathbf{r}))$.

[1] Folgar, F.P., C. Tucker, Orientation Behavior of Fibers in Concentrated Suspensions, Jn. of Reinforced Plastics and Composites **3** (1984) 98–119.

[2] Doi, M., Molecular Dynamics and Rheological Properties of Concentrated Solutions of Rodlike Polymers in Isotropic and Liquid Crystalline Phases, Jn. of Polymer Science Part B Polymer Physics **19** (1981) 229–243.

[3] Feng, J., L. Leal, Simulating Complex Flow of Liquid-Crystalling Polymers Using the Doi Theory, Journal of Rheology **41** (6) (1997) 1317–1335.

[4] Chaubal, C.V., L. Leal, A Closure Approximation for Liquid-Crystalline Polymer Models Based on Parametric Density Estimation, Journal of Rheology **42** (1) (1998) 177–201.

[5] Girimaji, S.S., A New Perspective on Realizability of Turbulence Models, Journal of Fluid Mechanics **512** (2004) 191–210.

[6] Forest, M.G., R. Zhou, Q. Wang, Nano-Rod Suspension Flows: A 2D Smoluchowski-navier-Stokes Solver, International Jounral of Numerical Analysis and Modeling **4** (3-4) (2007) 478–488.

[7] Upadhyay, R.R., O. Ezekoye, Treatment of Size-Dependent Aerosol Transport Processes Using Quadrature Based Moment Methods, Journal of Aerosol Science **37** (7) (2005) 799–819.

[8] Bird, R. B., C. Curtiss, R. C. Armstrong, O. Hassager, Dynamics of Polymeric Liquids, 2nd Edition, Vol. 2: Kinetic Theory, John Wiley & Sons, Inc., New York, NY, 1987.

[9] Petrie, C.J.S., The Rheology of Fibre Suspensions, Journal of Non-Newtonian Fluid Mechanics **87** (1999) 369–402.

[10] Advani, S.G., C. Tucker, The Use of Tensors to Describe and Predict Fiber Orientation in Short Fiber Composites, Jn. of Rheology **31** (8) (1987) 751–784.

[11] Altan, M.C., S. Subbiah, S. Guceri, R. Pipes, Numerical Prediction of Three-Dimensional Fiber Orientation in Hele-Shaw Flows, Polymer Engineering and Science **30** (14) (1990) 848–859.

[12] Cintra, J. S., C. Tucker, Orthotropic Closure Approximations for Flow-Induced Fiber Orientation, Jn. of Rheology **39** (6) (1995) 1095–1122.

[13] Jack, D.A., D. Smith, An Invariant Based Fitted Closure of the Sixth-order Orientation Tensor for Modeling Short-Fiber Suspensions, Jn. of Rheology **49** (5) (2005) 1091–1116.

[14] Nguyen, N., S. Bapanapalli, J. Holbery, M. Smith, V. Kunc, B. Frame, J. Phelps, C. Tucker, Fiber Length and orientation in Long-Fiber Injection-Molded Thermoplastics - Part I: Modeling of Microstructure and Elastic Properties, Jn. of Composite Materials **42** (10) (2008) 1003–1029.

[15] Koch, D.L., A Model for Orientational Diffusion in Fiber Suspensions, Physics of Fluids **7** (8) (1995) 2086–2088.

[16] Phan-Thien, N., X.-J. Fan, R. Tanner, R. Zheng, Folgar-Tucker Constant for a Fibre Suspension in a Newtonian Fluid, Journal of Non-Newtonian Fluid Mechanics **103** (2002) 251–260.

[17] Jack, D.A., Advanced Analysis of Short-fiber Polymer Composite Material Behavior, Ph.D. thesis, University of Missouri - Columbia (December 2006).

[18] Jack, D.A., S. Montgomery-Smith, D. Smith, Anisotropic Diffusion Model for Suspensions of Short-Fiber Composite Processes., in: The XVth International Congress on Rheology, the Society of Rheology 80th Annual Meeting, The Society of Rheology, Monterey, CA, 2008.

[19] Wang, J., J. O'Gara, C. Tucker, An Objective Model for Slow Orientation Kinetics in Concentrated Fiber Suspensions: Theory and Rheological Evidence, Journal of Rheology **52** (5) (2008) 1179–1200.

[20] Phelps, J.H., C. Tucker, An Anisotropic Rotary Diffusion Model for Fiber Orienation in Short- and LongFiber Thermoplastics, Journal of Non-Newtonian Fluid Mechanics **156** (2009) 165–176.

[21] Bay, R.S., C. Tucker, Fiber Orientation in Simple Injection Moldings: Part 2 - Experimental Results, in: Plastics and Plastic Composites: Material Properties, Part Performance, and Process Simulation, ASME 1991, Vol. **29**, American Society of Mechanical Engineers, 1991, pp. 473–492.

[22] Altan, M.C., S. Advani, S. Güçeri, R. Pipes, On the Description of the Orientation State for Fiber Suspensions in Homogeneous Flows, Jn. of Rheology **33** (7) (1989) 1129–1155.

[23] VerWeyst, B.E., C. Tucker, P. Foss, J. O'Gara, Fiber Orientation in 3-D Injection Molded Features: Prediction and Experiment, International Polymer Processing **14** (1999) 409–420.

[24] Chung, D.H., T. Kwon, Invariant-Based Optimal Fitting Closure Approximation for the Numerical Prediction of Flow-Induced Fiber Orientation, Jn. of Rheology **46** (1) (2002) 169–194.

[25] Han, K.-H., Y.-T. Im, Numerical Simulation of Three-Dimensional Fiber Orientation in Short-Fiber-Reinforced Injection-Molded Parts, Jn. of Materials Processing Technology **124** (2002) 366–371.

[26] Hand, G.L., A Theory of Anisotropic Fluids, Jn. of Fluid Mechanics **13** (1) (1962) 33–46.

[27] Verleye, V., F. Dupret, Prediction of Fiber Orientation in Complex Injection Molded Parts, in: Developments in Non-Newtonian Flows, 1993, pp. 139–163.

[28] Jack, D.A., D. Smith, Sixth-order Fitted Closures for Short-fiber Reinforced Polymer Composites, Jn. of Thermoplastic Composites **19** (2006) 217–246.

[29] Lipscomb, G G II., M. Denn, D. Hur, D. Boger, Flow of Fiber Suspensions in Complex Geometries, Jn. of Non-Newtonian Fluid Mechanics **26** (1988) 297–325.

[30] Jack, D.A., D. Smith, Assessing the Use of Tensor Closure Methods With Orientation Distribution Reconstruction Functions, Jn. of Composite Materials **38** (21) (2004) 1851–1872.

[31] Jack D.A., D. Smith, Elastic Properties of Short-Fiber Polymer Composites, Derivation and Demonstration of Analytical Forms for Expectation and Variance from Orientation Tensors, Journal of Composite Materials **42** (3) (2008) 277–308.

[32] Jack, D.A., D. Smith, The Effect of Fiber Orientation Closure Approximations on Mechanical Property Predictions, Composites, Part A **38** (2007) 975–982.

[33] Stewart, W.E., J. Sorensen, Hydrodynamic Interaction Effects in Rigid Dumbell Suspensions. II. Computations for Steady Shear Flow, Journal of Rheology **16** (1) (1972) 1–13.

[34] Bird, R.B., H. Warner, Hydrodynamic Interaction Effects in Rigid Dumbell Suspensions. I. Kinetic Theory, Journal of Rheology **15** (4) (1971) 741–750.

[35] Larson, R.G., Arrested Tumbling in Shearing Flows of Liquid Crystal Polymers, Macromolecules **23** (1990) 3983–3992.

[36] Larson, R.G., H. Öttinger, The Effect of Molecular Elasticity on Out-of-Plane Orientations in Shearing Flows of Liquid Crystalline Polymers, Macromolecules **24** (1991) 6270–6282.

[37] Vukadinovic, J., Inertial Manifolds for a Smoluchowski Equation on the Unit Sphere, Communications in Mathematical Physics **285** (2009) 975–990.

[38] Hinch, E.J., L. Leal, Time-Dependent Shear Flows of a Suspension of Particles with Weak Brownian Rotations, Journal of Fluid Mechanics **57** (1973) 753–767.

[39] Forest, M.G., Q. Wang, Monodomain Response of Finite-Aspect-Ratio Macromolecules in Shear and Related Linear Flows, Rheologica Acta **42** (2003) 20–46.

[40] Onat, E.T., Effective Properties of Elastic Materials that Contain Penny Shaped Voids, International Journal of Engineering Science **22** (8-10) (1984) 1013–1021.

[41] Onat, E.T., F. Leckie, Representation of Mechanical Behavior in the Presence of Changing Internal Structure, Jn. of Applied Mechanics **55** (1988) 1–10.

[42] Jeffery, G.B., The Motion of Ellipsoidal Particles Immersed in a Viscous Fluid, Proceedings of the Royal Society of London A **102** (1923) 161–179.

[43] Weisstein, E.W., Spherical Coordinates, Tech. rep., *Mathworld*–A Wolfram Web Resource, `http:// mathworld .wolfram .com/ SphericalCoordinates.html` (2008).

[44] Chung, D.H., T. Kwon, Improved Model of Orthotropic Closure Approximation for Flow Induced Fiber Orientation, Polymer Composites **22** (5) (2001) 636–649.

[45] VerWeyst, B.E., Numerical Predictions of Flow Induced Fiber Orientation in Three-Dimensional Geometries, Ph.D. thesis, University of Illinois at Urbana Champaign (1998).

[46] Bay, R.S., Fiber Orientation in Injection Molded Composites: A Comparison of Theory and Experiment, Ph.D. thesis, University of Illinois at Urbana-Champaign (August 1991).

Table 1: Comparison of the computational effort to solve the equation of motion given in wall-clock seconds.

	Hybrid	ORT	Spherical ($L = 50$)	Spherical ($L = 100$)	DFC
$t_{\text{Norm}}^{\text{Hi}}$	8.1×10^{-2}	1.4×10^{-1}	4.8×10^{-1}	1.8×10^{0}	3.5×10^{3}
$t_{\text{Norm}}^{\text{Mean}}$	7.3×10^{-2}	1.3×10^{-1}	4.3×10^{-1}	1.7×10^{0}	8.4×10^{2}
$t_{\text{Norm}}^{\text{Low}}$	7.0×10^{-2}	1.2×10^{-1}	3.7×10^{-1}	1.3×10^{0}	2.4×10^{1}

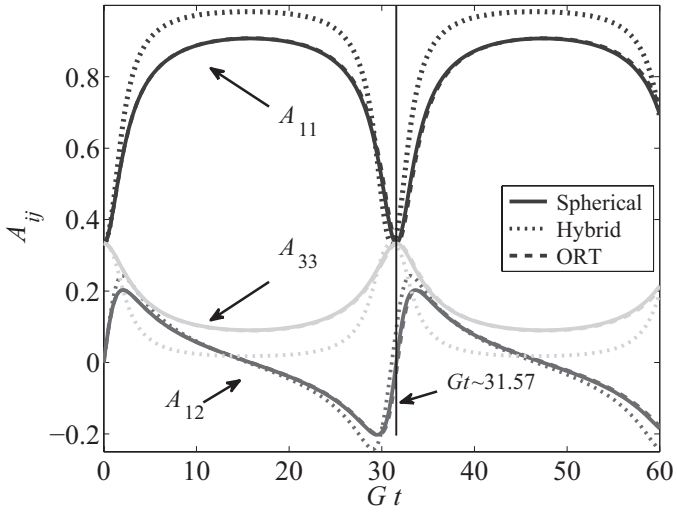

Figure 1: Results from numerical simulations of Jeffery's Equation, $\lambda = 0.98$.

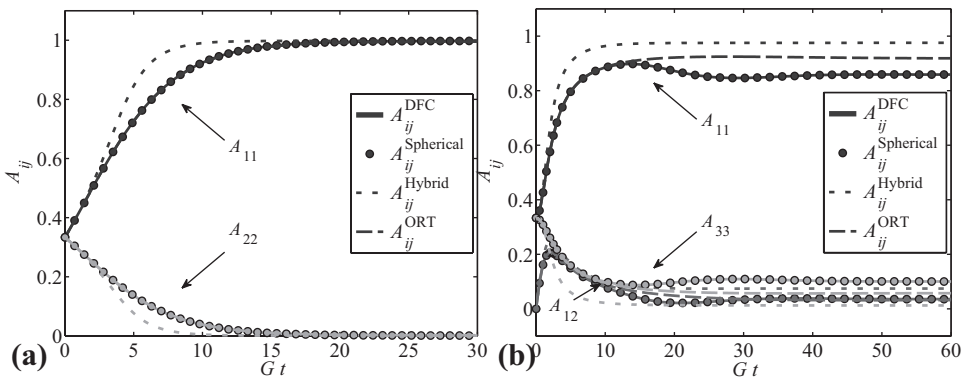

Figure 2: Results from numerical simulations of Jeffery's Equation with Folgar-Tucker Diffusion: DFC and Spherical Harmonic results, (a) Elongational flow, $C_I = 10^{-3}$, (b) Shear flow, $C_I = 10^{-3}$.

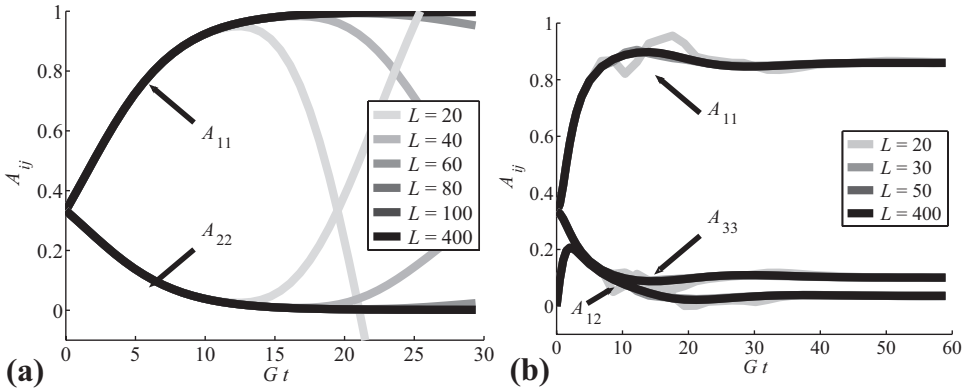

Figure 3: Results from numerical simulations of Jeffery's Equation with Folgar-Tucker Diffusion for increasing order of expansion: (a) Elongational flow, $C_I = 10^{-3}$, (b) Shear flow, $C_I = 10^{-3}$.

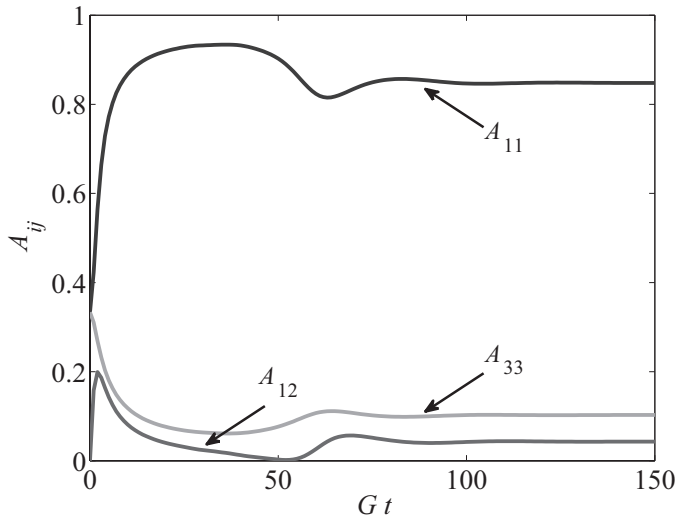

Figure 4: Results of numerical simulation of Jeffery's Equation with Koch diffusion, $v_f = 1\%$, $\lambda = 1$.

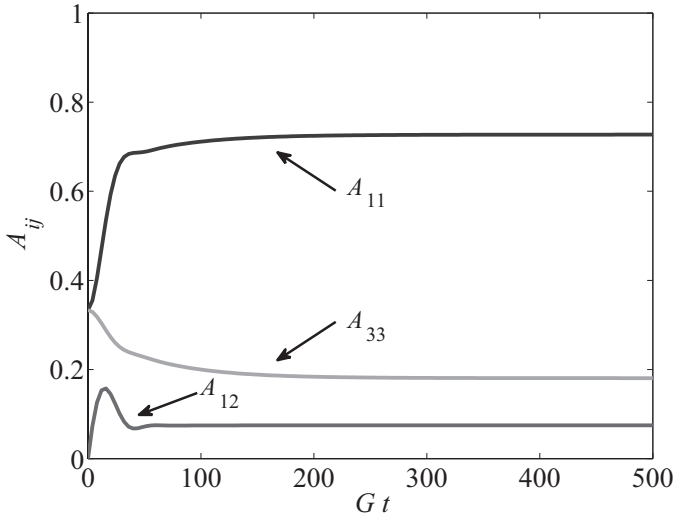

Figure 5: Results of numerical simulation of Jeffery's Equation with Folgar-Tucker diffusion and reduced-strain closure.

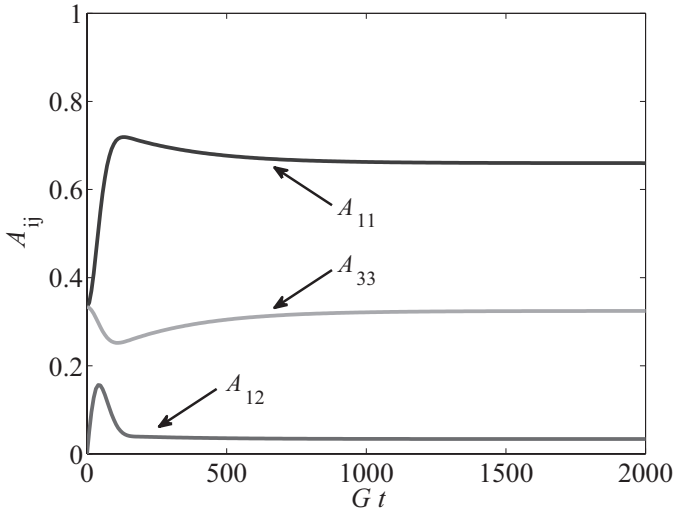

Figure 6: Results of numerical simulation of Jeffery's Equation with Phelps-Tucker anisotropic rotary diffusion, and reduced-strain closure.